Kasetsart J. (Nat. Sci.) 49 : 474 - 489 (2015)

Study of Sloshing of Viscous Liquid in Containers Using Finite Element Method

Noppadol Chaimanatsakun and Tumrong Puttapitukporn*

ABSTRACT

Severe liquid sloshing in moving partially-filled liquid containers following a sudden halt can generate enormous liquid pressure which can lead to vehicle accidents or damage to their internal structures. Many researchers have focused on studies of flow characteristics during the sloshing period using the fluid-structure interaction algorithm implemented in finite element analysis. The current research extended previous work to distinguish inviscid-flow models from viscous-flow models in simulations of liquid sloshing inside containers. Finite element models of water containers were developed consisting of containers with and without a water baffle. The water-filled capacities were set at 40, 60 and 80%. This research focused on analyses of surface waves, pressure waves and stress distribution on containers. When comparing inviscid-flow models to viscous-flow models at the same water-filled capacity, quite similar results were found in the shape of surface waves, maximum wave heights and the duration of occurrence of the peak von Mises stress. Nonetheless, inviscid-flow models had higher von Mises stress on the container surfaces than viscous-flow models. At 40% water-filled capacity, the water pressure randomly oscillated over time so that the peak water pressure could not be identified. The water baffle helped to minimize water pressures, heights of surface waves and von Mises stress on the container surfaces especially at 60 and 80% water-filled capacity.

Keywords: liquid sloshing, fluid-structure interaction, finite element analysis

NOMENCLATURE

$[M]$	Mass matrix
$[C]$	Damping matrix
$[K]$	Stiffness matrix
$\{D\}$	Displacement vector
$\left\{\dot{D}\right\}$	Velocity vector
$\left\{\ddot{D}\right\}$	Acceleration vector
$\{f_{ext}\}$	External load vector
ρ	Material density
u_i	Velocity components
p	Pressure
q	Bulk viscosity
g	Gravitational constant
e	Specific total energy
e_3	Unit vector in z-direction
V	Volume
A	Area
n_i	Normal vector along the surface area A
S_{ij}	Shear stress tensor
ρ	Overall material density
ρ_0	Reference density
a_1	Bulk modulus

Department of Mechanical Engineering, Faculty of Engineering, Kasetsart University, Bangkok 10900, Thailand.
* Corresponding author, e-mail: fengtop@ku.ac.th

Received date : 06/10/14 Accepted date : 28/03/15

INTRODUCTION

Liquid sloshing in partially-filled liquid containers is a consequence of the behavior of a liquid flowing inside moving containers. When these containers are suddenly stopped, immensely fluctuating pressure waves develop inside the containers which may damage their structures. Many researchers have studied sloshing behavior using the fluid-structure interaction (FSI) algorithm implemented in finite element analysis. In the FSI algorithm, the fluid inside a finite volume domain is bounded by a coupling surface which enables the fluid to exert a force onto deformable container structures. Kim (2001) studied the flow of liquid during the sloshing period in two dimensional (2D) and three dimensional containers using the finite difference method. Chen and Nokes (2005) examined the fully nonlinear free surface conditions of viscous fluid sloshing in a 2D rectangular container using the finite difference method. Rinker and Abatt (2006) demonstrated the capabilities and investigated the limitations of the MSC Dytran V.2006 program (MSC Software Corporation, 2005; Newport Beach, CA, USA) in performing dynamic fluid-structure analysis of the primary container and the contained waste. Here, artificial bulk viscosity was introduced as a linear bulk viscosity value of 0.2 and a quadratic bulk viscosity of 1.1. Suvanjumrat *et al.* (2008) studied drop tests of liquid-filled plastic containers to analyze the stress distribution on the containers using the MSC Dytran program. Lee *et al.* (2012) used the MSC Dytran program to investigate structures of breakwaters on container carriers under impact loads. Apinyamano *et al.* (2012) studied the effects of liquid sloshing in containers on their structural strength which was carried out by considering flow as inviscid.

MSC Dytran is a commercial software package for undertaking highly nonlinear transient analyses that involve structural and fluid parts. The fluid dynamics solver it contains uses an Eulerian approach and employs the finite volume method to discretize the governing equations. These equations are the conservation laws which are integrated in time by a first-order explicit algorithm.

The purpose of this research was to study the distinct characteristics of water sloshing inside moving containers when water is modeled as a viscous flow and an inviscid flow using the MSC Patran and MSC Dytran programs (MSC Software Corporation, 2005; Newport Beach, CA, USA). Containers with and without a water baffle were filled with water to 40, 60, and 80% of their maximum capacity. Containers with a water baffle were studied to minimize the severity of the water sloshing. The shapes and heights of surface waves, water pressures developed on the inner surfaces of containers and the stress distribution on container structures were analyzed.

MATERIALS AND METHODS

Numerical model

Liquid sloshing in containers can be analyzed using the nonlinear explicit finite element analysis in the MSC Dytran software which contains both a Lagrangian solver for computing structure dynamics and an Eulerian solver for computing fluid dynamics. In the Lagrangian solver, materials in Lagrangian meshes are fixed in constant mass elements and deformed with structures. The equation of motion is shown in Equation 1:

$$[M]\{\ddot{D}\}+[C]\{\dot{D}\}+[K]\{D\}=\{f_{ext}\} \quad (1)$$

In the Eulerian solver, materials in the Eulerian mesh can move from one constant volume element to the other. The equation for the conservation laws of mass is shown in Equation 2:

$$\frac{d}{dt}\int_V \rho dV+\int_A \rho(u\cdot n)dA=0 \quad (2)$$

The equation for the conservation law of momentum is shown in Equation 3:

$$\frac{d}{dt}\int_V \rho u_i dV + \int_A \rho u_i (u \cdot n) dA = -\int_A (p+q) n_i dA + \int_A s_{ij} n_j dA - \rho g e_3 V \quad (3)$$

The equation for the conservation law of energy is shown in Equation 4:

$$\frac{d}{dt}\int_V \rho e dV + \int_A \rho e (u \cdot n) dA = -\int_A u_i p n_i dA \quad (4)$$

The shear stress tensor S_{ij} given in Equation 3 is determined from Equation 5:

$$s_{ij} = \mu\left(e_{ij} - \frac{1}{3}e_{kk}\right) \quad (5)$$

where

$$e_{ij} = \frac{1}{2}\left(\frac{\partial u_i}{\partial x_j} + \frac{\partial u_j}{\partial x_i}\right)$$

To describe the state of the water, pressure p is written in the polynomial form as shown in Equation 7:

$$p = a_1\mu + a_2\mu^2 + a_3\mu^3 + (b_0 + b_1\mu + b_2\mu^2 + b_3\mu^3)\rho_0 e \quad (7)$$

where

$\mu = \rho / \rho_0 - 1$;
$a_2 = a_3 = 0$;
$b_1 = b_2 = b_3 = 0$

The air is considered as a void.

Bulk viscosity is an artificial viscosity introduced into the MSC Dytran program to control the formation of shock waves, to reduce oscillations of amplitude and to trail the shock front. The bulk viscosity can be defined by both linear bulk viscosity (BULKL) and quadratic bulk viscosity (BULKQ) which have default values of 0 and 1.0, respectively. Preliminary work determined that for water, a BULKL value of 0.1 yielded accurate finite element results compared to the experimental data of water pressure of Apinyamano *et al.* (2012). Therefore, in this research, the bulk viscosity was set at BULKL = 0.1 and BULKQ = 1.0.

In FSI, the fluid inside a finite volume domain is bounded by coupling surfaces. On these coupling surfaces, the interaction between fluids and structures can be calculated by the general coupling algorithm. This algorithm is used to compute interactions between Lagrangian and Eulerian elements. As the grid points of Lagrangian elements are moved, the Eulerian elements have a new boundary. The mass in the Eulerian elements exerts pressure on the Lagrangian elements which results in new grid points of the acceleration and velocity of structures. Updated plastic strains or stresses in the Lagrangian elements are used to determine whether or not these elements are failing. Finally, the Lagrangian grid points are moved with the new velocities.

Finite element models

The MSC Patran program was used to create models of the container and water while the MSC Dytran program was used as the solver. Nine case studies were analyzed. Case studies 1–3 were containers without the water baffle—inviscid-flow models—with 40, 60, and 80% water-filled capacities, respectively. Case studies 4–6 were containers without the water baffle—viscous-flow models—with 40, 60 and 80% water-filled capacities, respectively. Finally, case studies 7–9 were containers with the water baffle—viscous-flow models—with 40, 60 and 80% water-filled capacities, respectively. The dimensions of the containers were 131 mm width, 166 mm height, 256 mm length with walls of 6 mm thickness. For the container with the water baffle, the water baffle was installed at the middle of the container and was made of the same material as the containers. The dimensions of the baffle were 131 mm width, 166 mm height and 6 mm thickness. A circular hole at the center of the baffle (85 mm diameter) constituted 30% of the total baffle area.

Container models

Containers were modeled in the MSC Patran program using quadrilateral shell elements. The top surface of containers was closed by a

cover plate which was modeled using quadrilateral dummy elements. These dummy elements did not have stiffness and only needed to close a container volume. For containers with water baffles, the container and water baffle were modeled using quadrilateral shell elements and a hole at the center of the water baffle was modeled as quadrilateral dummy elements to define the flow connections between the two domains. All mesh sizes of the containers and the water baffle were 0.005 × 0.005 m. The structural meshes of containers without and with the water baffle are shown in Figure 1. Both the container and water baffle were made of an acrylic material with a density of 1,180 kg.m^{-3}, Young's modulus of 2.88 GPa, Poisson's ratio of 0.402 and a yield strength of 73.7 MPa (MatWab, LLC, 1996).

Fluid models

To model water inside the container, the Euler domain was created using the mesh generator algorithm to define the boundary and to create the mesh for the Euler domain. The Euler domain was modeled using hexahedron Eulerian elements having a mesh size of 0.005 × 0.005 × 0.005 m. Both water and void were contained inside the Euler domain. The material properties of water were a bulk modulus of 2.2 GPa, reference density of 1,000 kg.m^{-3}, dynamics viscosity of 0.89 mPa.s (at 25 °C). The Euler domain of the container without a water baffle is shown in Figure 2a. The coupling surface generated from the general coupling algorithm is indicated as the region of fluid (water and void) and was the boundary of the FSI.

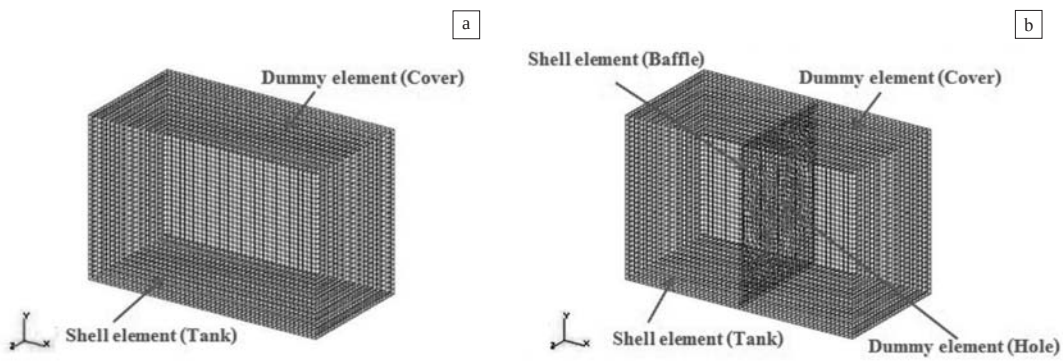

Figure 1 Structural meshes of containers: (a) Container without water baffle; (b) Container with water baffle.

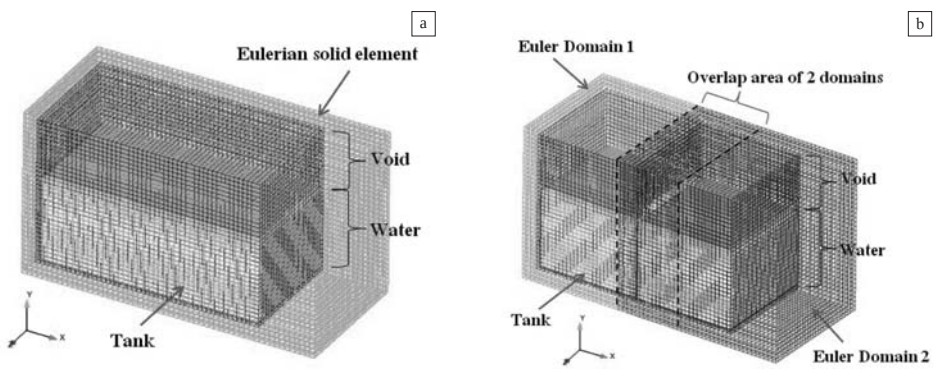

Figure 2 Euler domain meshes: (a) Container without the water baffle, (b) Container with the water baffle.

Inside the container with the water baffle, two Euler domains were created to separate the front volume from the rear volume of the container and these had to partially overlap as shown in Figure 2b. The elements at a middle hole were defined as porosity using the coupling porosity algorithm to connect the flow of water between these two domains. These elements must be included in the definition of couple surfaces.

Initial and boundary conditions

The initial conditions of the containers were defined in the Euler domain to fill water to 40, 60 and 80% of their maximum capacities. The Euler domain was associated with the coupling surface to create the region of fluid inside the containers. The initial velocity of the containers and water was 0.4 $m.s^{-1}$ in *x*-direction. Motion of containers was controlled by their bottom surfaces with the velocity versus time as shown in Figure 3.

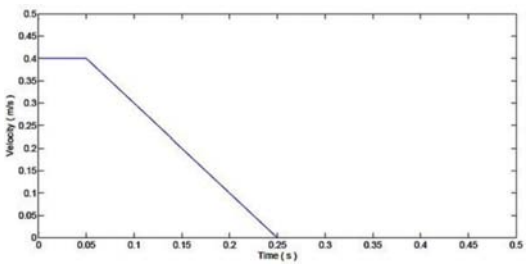

Figure 3 Boundary velocity in *x*–direction of all structural nodes located on the bottom surface of containers.

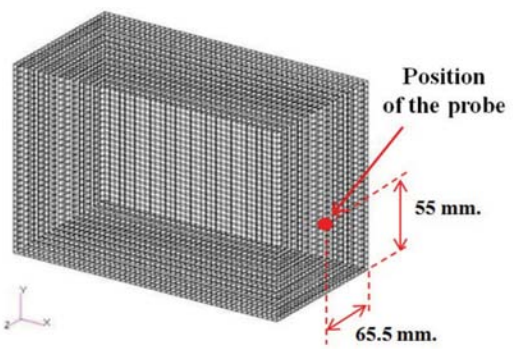

Figure 4 Position of probe for acquiring finite element results.

RESULTS AND DISCUSSION

Figure 4 shows the probe position for inquiring finite element results located at the front surface of a container. Figure 5 shows the water pressure measured at the probe for case studies 1–3 (containers without the water baffle and an inviscid-flow model at 40, 60 and 80% water-filled capacities). It was found that these water pressures randomly oscillated over time so that the sloshing characteristics could not be identified.

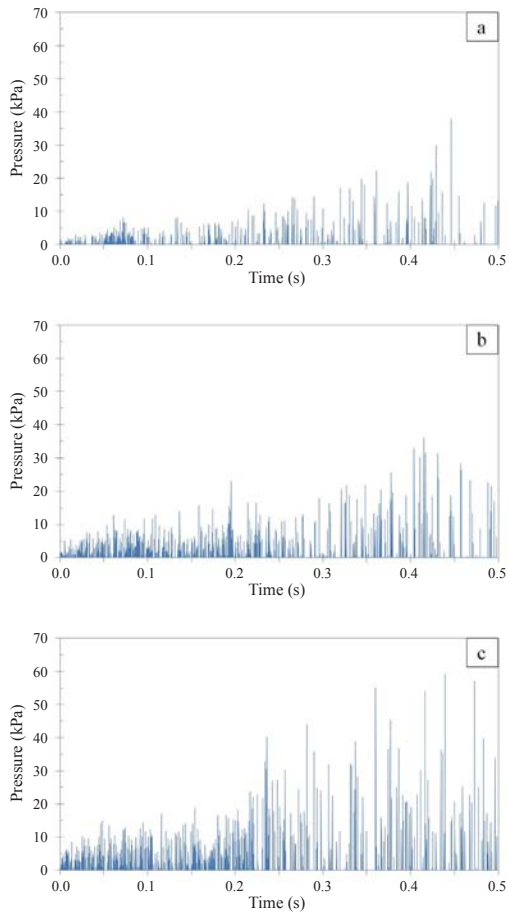

Figure 5 Finite element results of water pressures at the probe for case studies 1–3 (containers without water baffle and inviscid-flow model): (a) 40% water-filled capacity; (b) 60% water-filled capacity; (c) 80% water-filled capacity.

Figure 6 shows water pressure measured at the probe for case studies 4–6 (containers without the water baffle and a viscous-flow model at 40, 60 and 80% water-filled capacities). Here, the water properties were modeled with a bulk viscosity (BULKL = 0.1 and BULKQ = 1.0). To minimize noises in the pressure data, these finite element results were filtered using both the fast Fourier transform (FFT) and low-pass filters in the Matlab program (MathWork; Natick, CA, USA). Figure 7 shows the filtering process of water pressure

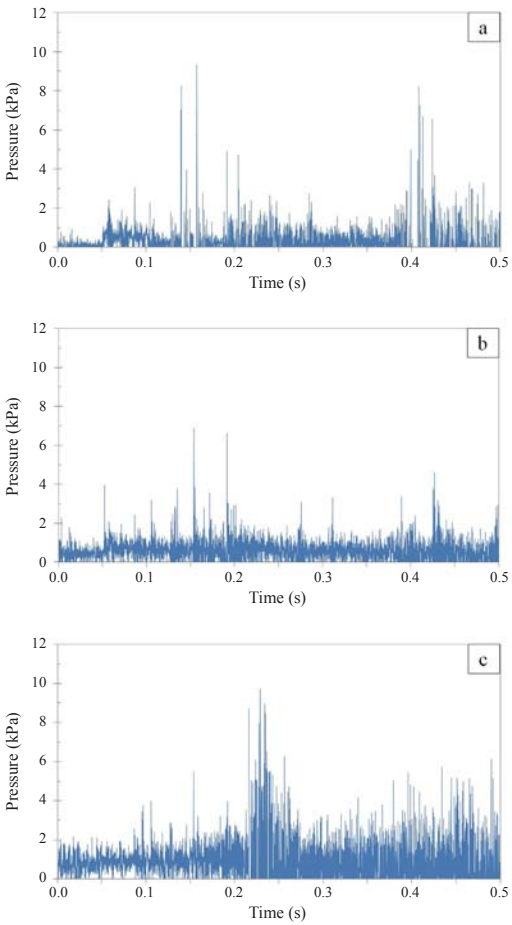

Figure 6 Finite element results of water pressures at the probe for case studies 4–6 (containers without water baffle and viscous-flow model): (a) 40% water-filled capacity; (b) 60% water-filled capacity; (c) 80% water-filled capacity.

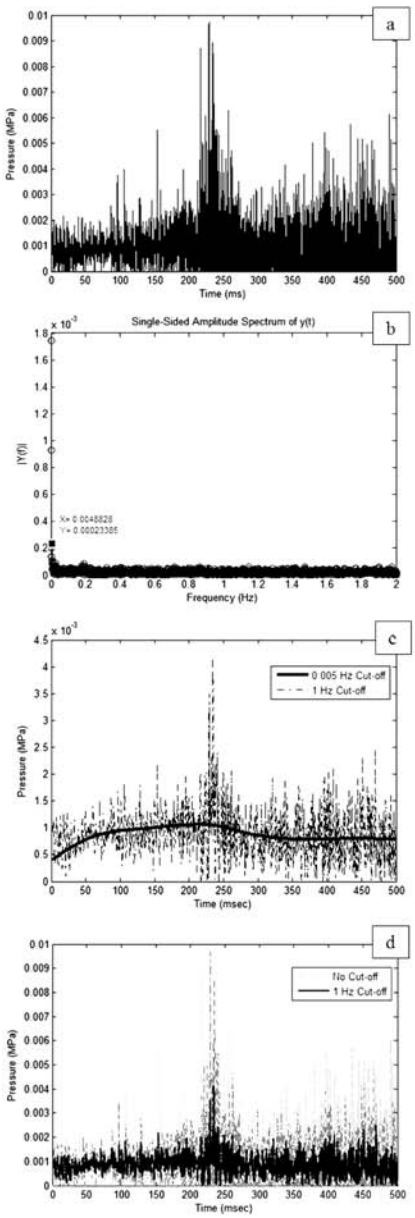

Figure 7 Filtering process of water pressure data of case study 6 using fast Fourier transform (FFT) and low-pass filters: (a) Water pressure versus time; (b) Amplitude spectrum versus time using FFT; (c) Comparison of water pressure versus time filtered at f_c = 0.005 and 1 Hz; (d) water pressure versus time of unfiltered and filtered water pressure data (at f_c = 1 Hz).

data for case study 6 using the FFT and low-pass filters. Figure 7b shows the cut-off frequency (f_c) of 0.005 Hz obtained from the FFT. The sampling frequency (f_s) of the water pressure data was 10 Hz and the Nyquist frequency ($f_{nyquist}$) was $f_s/2$ = 5 Hz. Consequently, the normalized cut-off frequency (f_{norm}) was 0.001 Hz. Figure 7c shows water pressure versus time of filtered data at cut-off frequencies of 0.005 and 1 Hz (determined by verifying maximum water pressure with the experimental data of Apinyamano *et al.* (2012)). Figure 7d shows the comparison of water pressure versus time of raw and filtered data.

Figures 8–9 show plots of filtering data of water pressure versus time at the probe for case studies 4–9 which were the containers without the water baffle and with the water baffle, respectively. The viscosity of water was modeled as BULKL = 0.1 and BULKQ = 1.0. As the water-filled capacity increased, the pressure increased. For containers without the water baffle and containers with the water baffle at 60 and 80% water-filled capacities, the peak pressure could be identified but at 40%

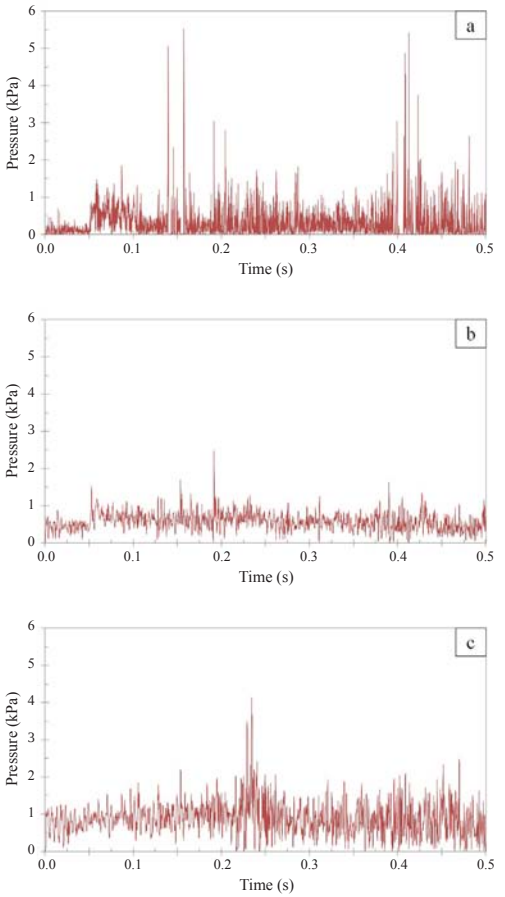

Figure 8 Finite element results of water pressure at the probe for case studies 4–6 (containers without water baffle and viscous-flow model): (a) 40% water-filled capacity; (b) 60% water-filled capacity; (c) 80% water-filled capacity.

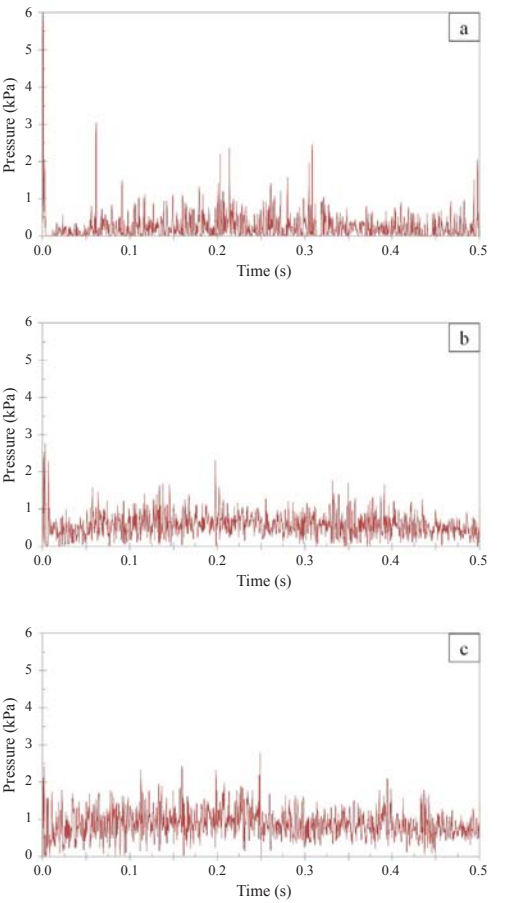

Figure 9 Finite element results of the pressure at the probe for case studies 7–9 (containers with water baffle and viscous-flow model): (a) 40% water-filled capacity; (b) 60% water-filled capacity; (c) 80% water-filled capacity.

water-filled capacity, randomly oscillating pressure remained.

Figures 10–12 show plots of von Mises stress versus time acquired at the probe for the nine case studies. As the water-filled capacity increased, the von Mises stress also increased. In all case studies, von Mises stresses increased substantially when the brake was initially applied at $t = 0.05$ s. During time 0.05–0.25 s (the braking period), von Mises stress continuously increased due to the effects of water sloshing until the container stopped moving. After the container was completely stationary, von Mises stress tended to decrease. During $t = 0$–6 ms in case studies 7–9 (the container with the water baffle and viscous-flow models), the water pressure and von Mises stress at the probe showed a spike as results of numerical errors as shown in Figure 13. Figure 13 shows the velocity versus time inquiring from the node located on the bottom surface of the container whose velocity was bounded by the boundary velocity.

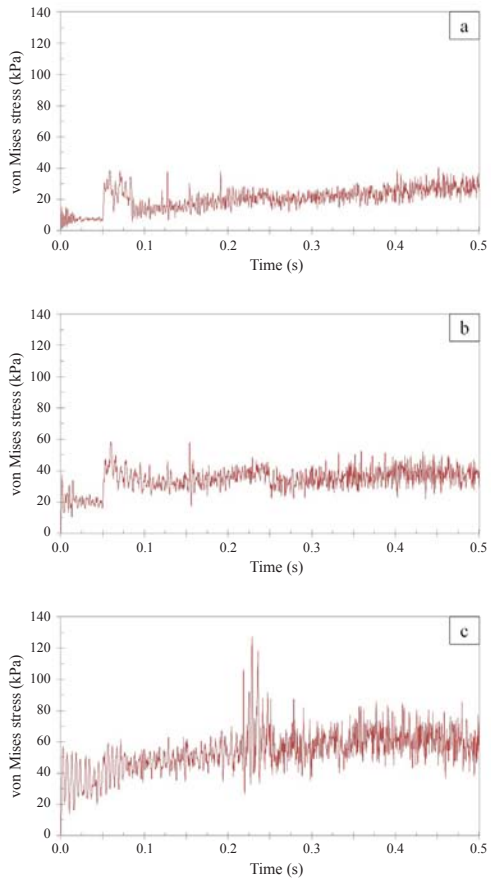

Figure 10 Finite element results of von Mises stress at the probe for case studies 1–3 (containers without water baffle and inviscid-flow model): (a) 40% water-filled capacity; (b) 60% water-filled capacity; (c) 80% water-filled capacity.

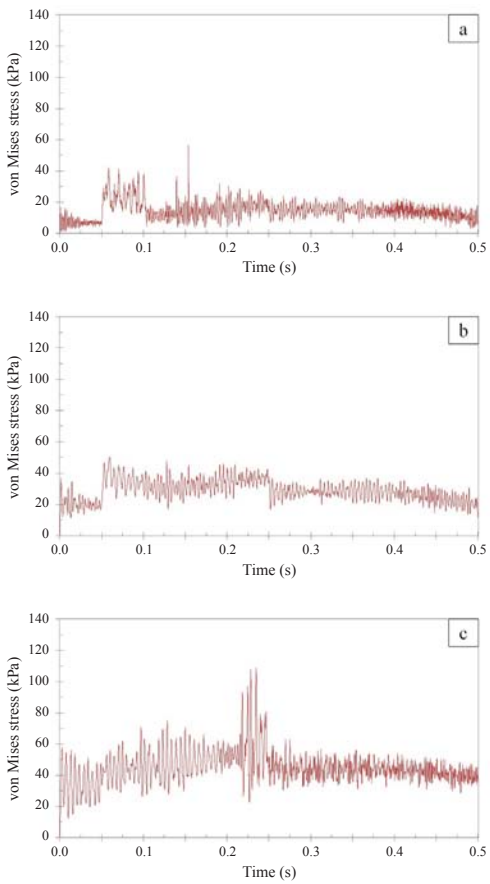

Figure 11 Finite element results of von Mises stress at the probe for case studies 4–6 (containers without water baffle and viscous-flow model): (a) 40% water-filled capacity; (b) 60% water-filled capacity; (c) 80% water-filled capacity.

Tables 1–3 show the shapes of surface waves of water for case studies 1–9 comparing the finite element results to the experimental results. The heights of surface waves on the front surface during sloshing periods for case studies 1–9 are shown in Tables 4–6. Shapes of surface waves during sloshing periods of the inviscid-flow model were similar to those of the viscous-flow model. Compared to the experimental results, the finite element results of the heights of surface waves had errors less than 20% for case studies 1–6 (the container without the water baffle) and less than 10% in case studies 7–9 (the container with the water baffle).

Figure 14 shows the comparison of von Mises stress distribution on container surfaces at time 0.25 s for case studies 1–9. Figure 15 shows the comparison of the plot of the maximum von Mises stress on the container versus time for case studies 1–9. As the water-filled capacity increased, von Mises stress also increased. Inviscid-flow models had the maximum von Mises stress—higher than in the viscous-flow models. At water-filled capacities of 60 and 80%, the containers with the water baffle could reduce the maximum von Mises stress on the container surfaces. However, at 40% water-filling capacity, no effect of the water baffle on the maximum von Mises stress on container surfaces was observed.

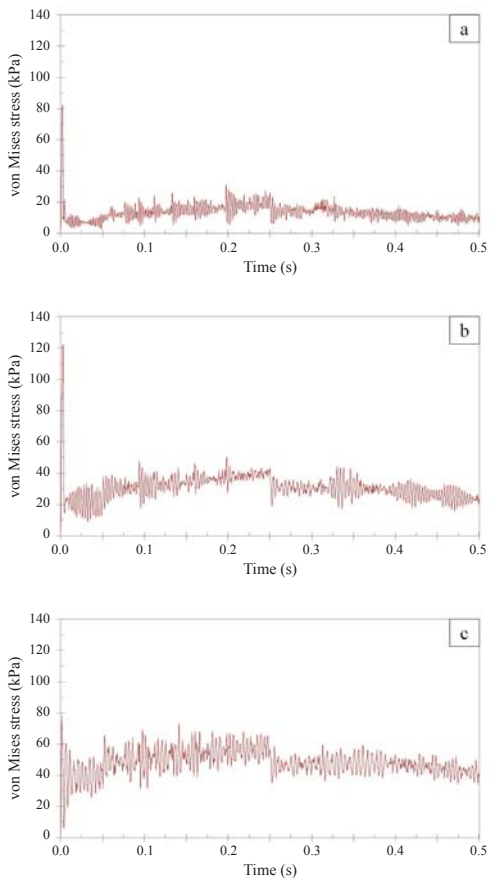

Figure 12 Finite element results of von Mises stress at the probe for case studies 7–9 (containers with water baffle and viscous-flow model): (a) 40% water-filled capacity; (b) 60% water-filled capacity; (c) 80% water-filled capacity.

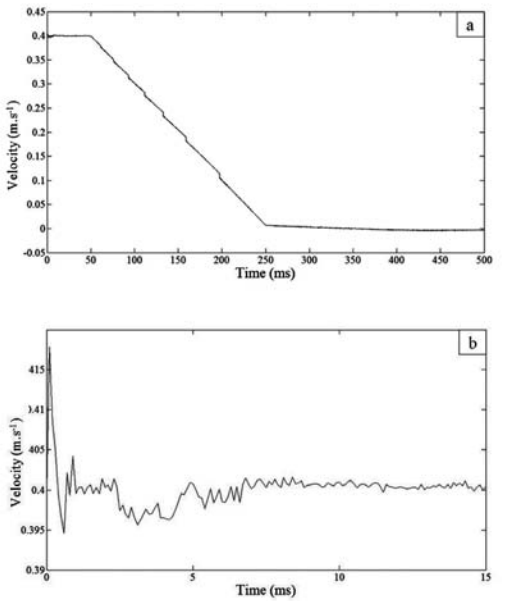

Figure 13 Plot of velocity versus time at the node located on the bottom surface of the container which was bounded by the boundary velocity: (a) $0 \leq t \leq 500$ ms; (b) $0 \leq t \leq 15$ ms.

Table 1 Comparison of shapes of surface waves of water during sloshing at 40% water-filledcapacity.

Time (s)	Container without water baffle			Container with water baffle	
	Experiment	Inviscid-flow model	Viscous-low model	Experiment	Viscous-flow model
0		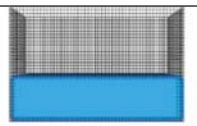	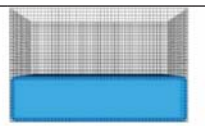		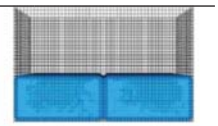
0.05	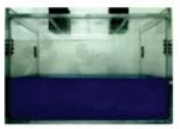	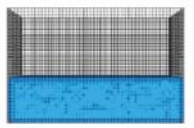	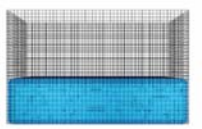	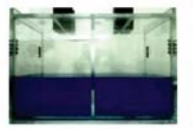	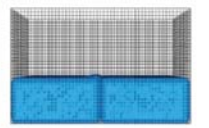
0.1		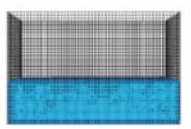	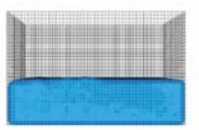		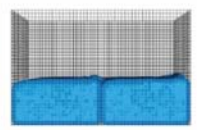
0.2		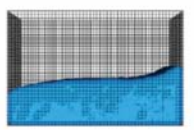	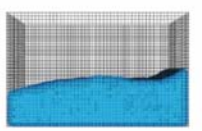		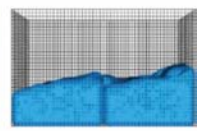
0.25	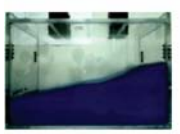	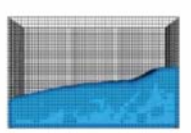	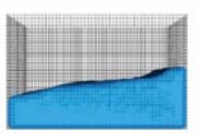		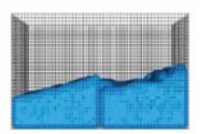
0.3		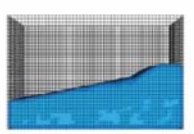	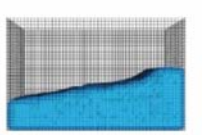		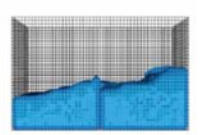
0.4	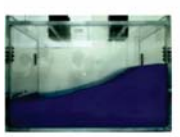	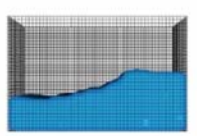	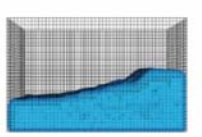	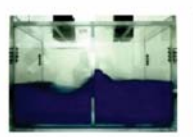	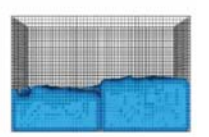
0.5		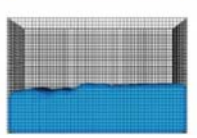	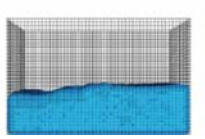	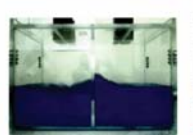	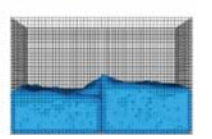

Table 2 Comparison of shapes of surface waves of water during sloshing at 60% water-filledcapacity.

Time (s)	Container without water baffle			Container with water baffle	
	Experiment	Inviscid-flow model	Viscous-low model	Experiment	Viscous-flow model
0		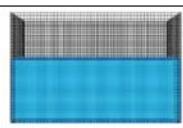	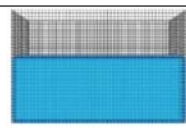		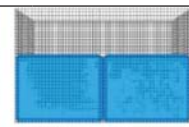
0.05		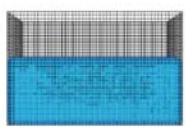	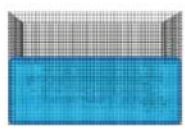	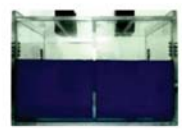	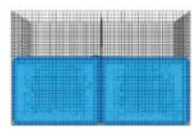
0.1		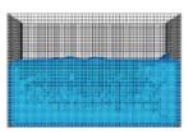	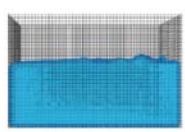		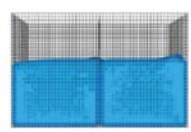
0.2		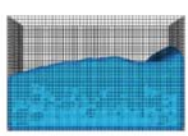	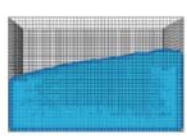		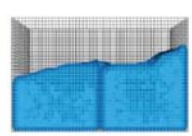
0.25		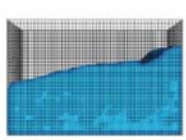	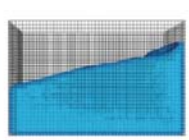		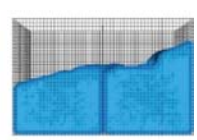
0.3		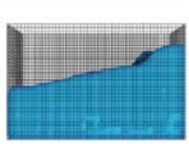	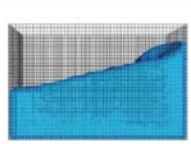		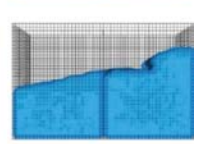
0.4		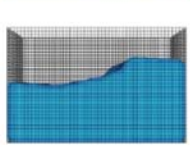	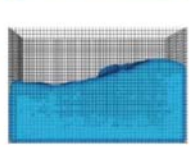		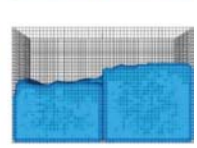
0.5			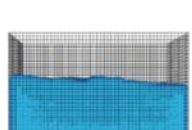		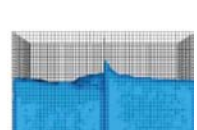

Table 3 The comparison of shapes of surface waves of water during sloshing at 80% water-filled capacity.

Time (s)	Container without water baffle			Container with water baffle	
	Experiment	Inviscid-flow model	Viscous-low model	Experiment	Viscous-flow model
0					
0.05	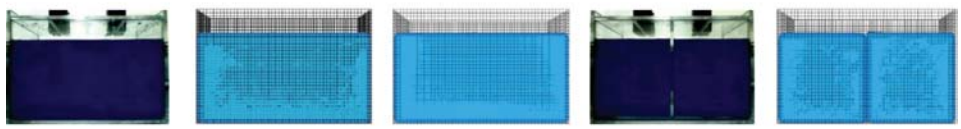				
0.1	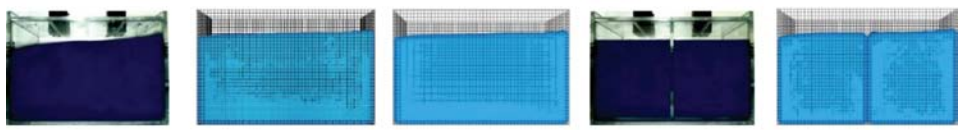				
0.2	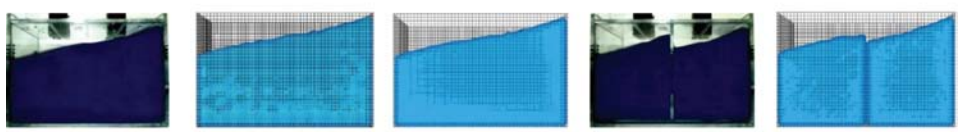				
0.25	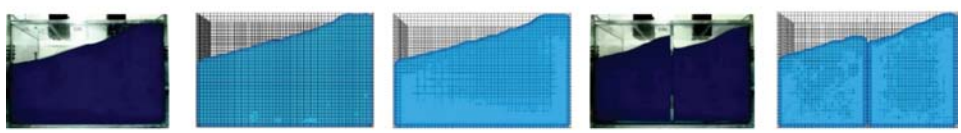				
0.3	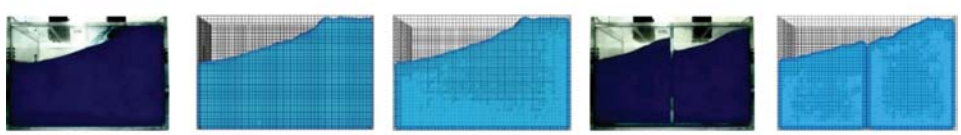				
0.4	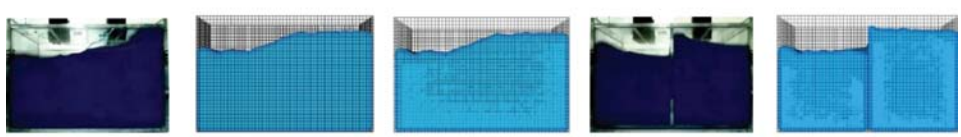				
0.5	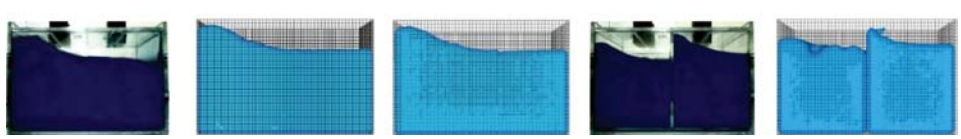				

Table 4 Heights of surface waves on the front surface of containers at 40% water-filled capacity.

Tim (s)	Container without water baffle					Container with water baffle		
	Experiment (m)	Inviscid-flow model		Viscous-flow model		Experiment (m)	Viscous-flow model	
		FEM (m)	Error (%)	FEM (m)	Error (%)		FEM (m)	Error (%)
0	0.064	0.064	0.00	0.064	0.00	0.064	0.064	0.00
0.05	0.064	0.064	0.00	0.064	0.00	0.064	0.064	0.00
0.1	0.065	0.065	0.00	0.064	-1.54	0.071	0.072	0.85
0.2	0.074	0.084	12.97	0.082	10.27	0.090	0.087	-3.78
0.25	0.097	0.091	-6.60	0.088	-9.69	0.090	0.092	1.78
0.3	0.097	0.093	-4.54	0.091	-6.60	0.089	0.094	5.17
0.4	0.099	0.084	-15.56	0.083	-16.57	0.079	0.077	-3.04
0.5	0.078	0.069	-12.05	0.070	-10.77	0.067	0.067	-0.60

FEM = Finite element model.

Table 5 Heights of surface waves on the front surface of containers at 60% water-filled capacity.

Time (s)	Container without water baffle					Container with water baffle		
	Experiment (m)	Inviscid-flow model		Viscous-flow model		Experiment (m)	Viscous-flow model	
		FEM (m)	Error (%)	FEM (m)	Error (%)		FEM (m)	Error (%)
0	0.096	0.096	0.00	0.096	0.00	0.096	0.096	0.00
0.05	0.096	0.096	0.00	0.096	0.00	0.096	0.096	0.00
0.1	0.100	0.107	7.40	0.106	6.40	0.102	0.103	1.37
0.2	0.115	0.123	7.30	0.120	4.70	0.114	0.123	8.25
0.25	0.128	0.131	2.66	0.134	5.00	0.126	0.131	4.29
0.3	0.133	0.133	0.30	0.141	6.32	0.126	0.129	2.70
0.4	0.120	0.115	-3.83	0.118	-1.33	0.119	0.111	-6.39
0.5	0.085	0.096	13.41	0.093	9.88	0.098	0.098	0.41

FEM = Finite element model.

Table 7 shows comparisons of the simulation time in each case study. For the container without the water baffle, viscous-flow models consumed 18–23% higher central processing unit time than the inviscid-flow models.

CONCLUSION

Viscous-flow models of water in moveable containers during the sloshing period were effective in analysis using the general coupling method in the MSC Dytran program. The water pressures, heights of the surface wave and von Mises stress distribution on the container surfaces were studied to distinguish the sloshing characters of viscous-flow models from inviscid-flow models. When comparing inviscid-flow models to viscous-flow models at the same water-filled capacity, the results were the same in the shapes and heights of surface waves and the durations of occurrence of the peak von Mises stress. Inviscid-flow models had higher von Mises stress on the container surfaces than the viscous-flow models. However, at 40% water-filled capacity, the water pressure randomly oscillated over time so that the peak pressure could not be identified. The water baffle helped to minimize water pressures, heights of surface waves and von Mises stress on the container surfaces, especially at 60 and 80% water-filled capacities.

Table 6 Heights of surface waves on the front surface of containers at 80% water-filled capacity.

Time (s)	Container without water baffle					Container with water baffle		
	Experiment (m)	Inviscid-flow model		Viscous-flow model		Experiment (m)	Viscous-flow model	
		FEM (m)	Error (%)	FEM (m)	Error (%)		FEM (m)	Error (%)
0	0.128	0.128	0.00	0.128	0.00	0.128	0.128	0.00
0.05	0.128	0.128	0.00	0.128	0.00	0.128	0.128	0.00
0.1	0.129	0.133	3.26	0.133	3.26	0.129	0.133	3.26
0.2	0.156	0.156	0.13	0.156	0.13	0.150	0.154	2.80
0.25	0.160	0.160	0.00	0.160	0.00	0.155	0.160	3.35
0.3	0.160	0.160	0.00	0.160	0.00	0.155	0.160	3.35
0.4	0.160	0.141	-11.75	0.141	-11.75	0.144	0.142	-1.25
0.5	0.123	0.119	-3.09	0.119	-3.09	0.122	0.126	3.44

FEM = Finite element model.

Table 7 Comparison of the simulation time of each case study.

Case study number	Simulation time (hr)		
	Water-filled capacity		
	40%	60%	80%
1–3	17	15	13
4–6	20	18	16
7–9	40	37	34

Computer processing unit: Intel® Core™ i5-3570 CPU @ 3.40GHz, RAM: DDR3-1600 16.0 GB.

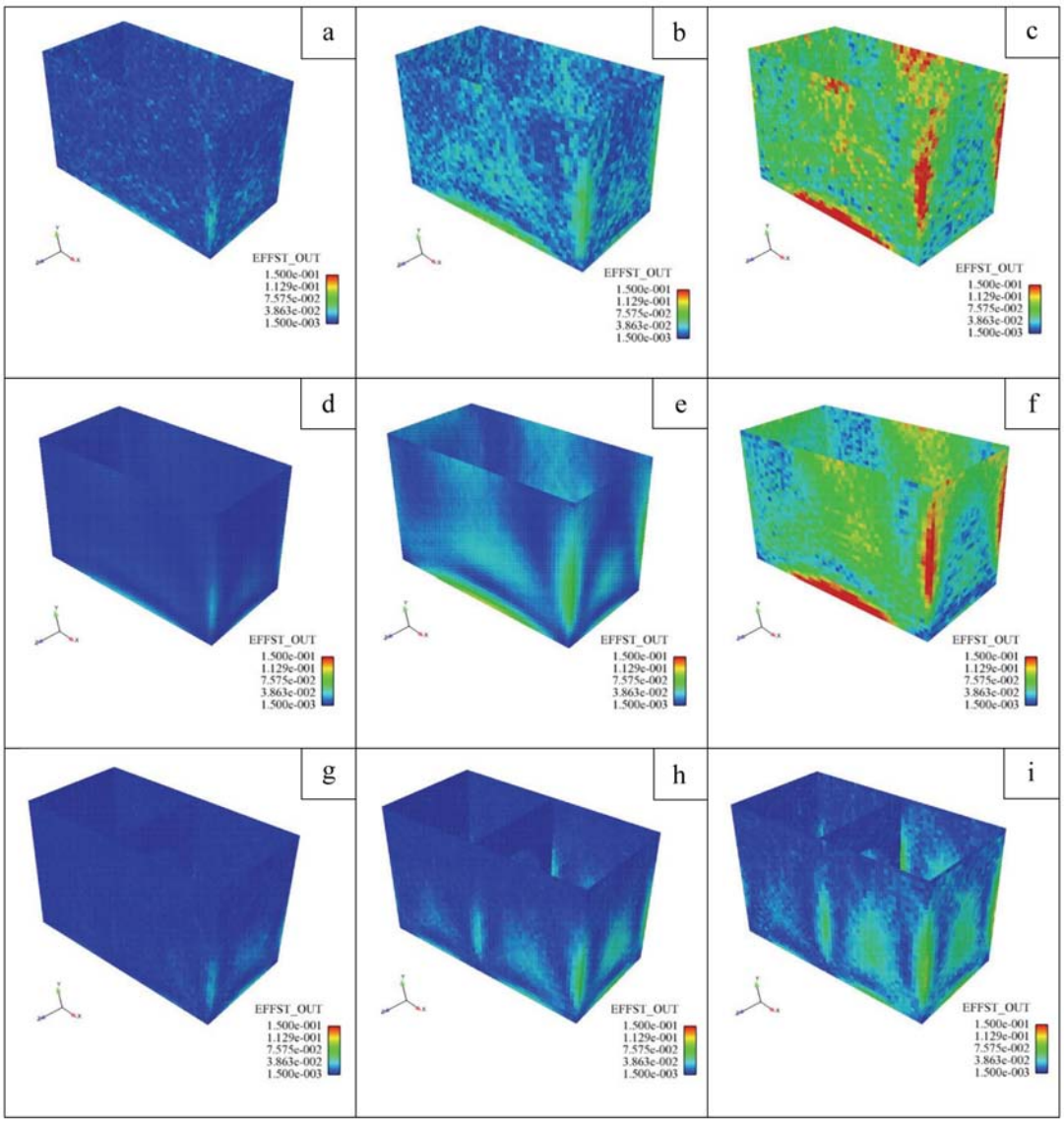

Figure 14 Von Mises stress distribution (MPa) on container surfaces at t = 0.25 s: (a) Case study 1; (b) Case study 2; (c) Case study 3; (d) Case study 4; (e) Case study 5; (f) Case study 6; (g) Case study 7; (h) Case study 8; (i) Case study 9.

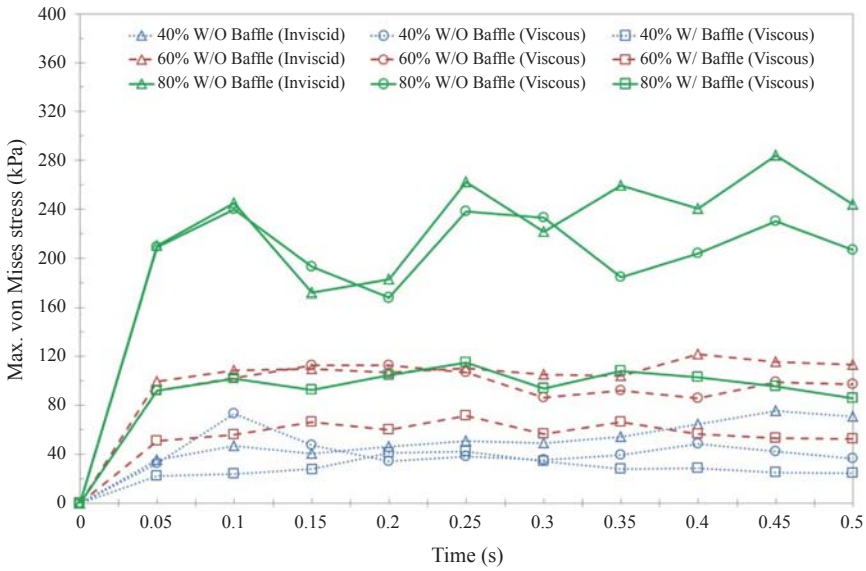

Figure 15 Comparison of the maximum (Max.) von Mises stress on container surfaces versus time for case studies 1–9. (W/O = Without; W/ = With.)

LITERATURE CITED

Apinyamano, W., T. Puttapitukporn and V. Juntasaro. 2012. A study of effects of liquid sloshing in a container on its structural strength. *In* **The 50th Kasetsart University Annual Conference on Architecture and Engineering)** 31 January–2 February 2012, Bangkok, Thailand. 7 pp.

Chen, B.F. and R. Nokes. 2005. Time-independent finite difference analysis of fully non-linear and viscous fluid sloshing in a rectangular container. **J. Comput. Phys.** 209: 47–81.

Kim, Y. 2011. Numerical simulation of sloshing flows with impact load. **Appl Ocean Res.** 23: 53–62.

Lee, C.H., H.S. Heo, Y.N. Kim, M.H. Kim, S.H. Kim and J.M. Lee. 2012. Investigation of structural responses of breakwaters for green water based on fluid-structure interaction analysis. **Inter. J. Nav. Archit. Oc. Engng.** 4: 83–95.

MatWeb, L.L.C. 1996. **Overview of Materials for Acrylic, Extruded.** [Available from: http://www.matweb.com/search/DataSheet.aspx?MatGUID=632572aeef2a4224b5ac8fbd4f1b6f77&ckck=1]. [Sourced: 10 September 2014].

MSC. Software. 2005. **MSC.Dytran Theory Manual.** MSC. Software Corporation. Newport Beach, CA, USA.

Rinker, M.W. and F.G. Abatt. 2006. **Dytran Analysis of Seismically Induced Fluid Structure Interaction in a Hanford Double-Shell Primary Container.** Pacific Northwest National Laboratories. Richland, WA, USA. 208 pp.

Suvanjumrat, C., T. Puttapitukporn and S.Thusneyapan. 2008. Analysis of fluid-structure interaction effects of liquid-filled container under drop testing. **Kasetsart J. (Nat. Sci.)** 42: 165–176.